11th International Workshop on Ship and Marine Hydrodynamic
Hamburg, Germany, September 22-25, 2019

A Potential Method for Fully Non-Linear Wave Responses of Ships

Heinrich Söding

Hamburg University of Technology, Institute for Fluid Dynamics and Ship Theory
Am Schwarzenberg-Campus 1, 21073 Hamburg, Germany

*Corresponding author, h.soeding@gmx.de

ABSTRACT

Existing methods to compute wave motions of and loads on ships either neglect effects depending non-linearly on wave height (linear boundary-element methods), or they take too much preparation and computing time for most practical applications (field methods solving Euler or RANS equations), or they take into account only some, but not all substantial non-linear effects (non-linear potential methods), or they are suitable only for strongly simplified hull shapes like Wigley ships. Here a potential method is described which avoids the listed deficiencies of existing potential methods while being much faster than field methods. Many new or seldom-applied features were required to attain that goal. To list here only a few of them: Instead of resolving splashes and wave breaking at the waterline, emphasis is laid on avoiding instabilities while skipping these flow details. The total flow potential is added from that of the undisturbed wave and the disturbance; this allows damping of the latter to avoid wave reflections at the outer boundary while leaving the incoming wave unaffected. Time derivatives of the potential ϕ are determined by computing both ϕ and $\dot{\phi}$ from the respective boundary conditions. The method is verified by comparisons with model experiments and different kinds of computations.

1 INTRODUCTION

The success of linear strip and panel methods for motion and load predictions motivated many attempts to improve these methods by considering effects depending non-linearly on wave and/or motion amplitude. Especially the roll motion and the accompanied torsional moment are severely influenced by non-linear effects caused, besides others, by the deviation of the righting arm curve from a straight line, and by parametric excitation. Of much practical interest is also the difference between the absolute value of the vertical wave-induced bending moment (and shear force) between wave crest and trough condition, a non-linear effect caused by variations of the hull immersion at both ends. As a first improvement of linear methods, the integration of hull pressure to obtain the pressure force and moment is extended in many non-linear methods up to the actual instead of up to the mean waterline. Depending on details of the implementation, on the response of interest and on wave frequency and direction, this may or may not result in improvements. Many terms in the computations nearly cancel each other. For instance in long waves, where the ship nearly follows the wave motion, radiation and wave-induced forces nearly cancel. Thus, improving the accuracy of either wave or radiation force, but not of both, will increase inaccuracies at least in some wave conditions. The same holds for Froude-Krilow and diffraction pressures at the ship's bottom, which nearly cancel in short waves.

Thus, it is tried here to model all substantial non-linear wave and motion effects. To attain that goal by a boundary-element method, only Rankine source methods appear suitable. In these, the submerged part of the hull and a finite region of the water surface around the ship are covered by source and/or dipole panels to model the flow around the ship, which determines the hull pressure and, thus, force and motion.

Special difficulties with non-linear Rankine panel codes are:

- Large motions between water surface and body cause corresponding motions between the body and the free-

surface panel mesh. A free-surface mesh extending into the body would give inaccurate results. Thus the free-surface panel mesh must follow the waterline. For typical ship shapes, this involves also topological mesh changes especially if a transom stern changes from immersed to emerged.

- Surface irregularities like breaking waves and spray form at the waterline, especially in upward relative motion of the water along flaring sections. Because they cannot be resolved by a reasonably coarse panel mesh, they must be skipped somehow, without causing a failure of the simulation.

At the moment, the method is confined to rigid symmetrical single-hull ships in deep water with or without forward speed. Cases with an immersed weather deck may cause difficulties.

2 COORDINATE SYSTEMS

3 different coordinate systems are used:

- An inertial system having its origin at the mean water surface. In most methods it follows the mean forward speed of the vessel; however, if maneuvering in waves should be included, there is no mean forward speed. Thus here the system is earth-fixed or – in case of a steady homogeneous current – it follows the current flow. Inertial coordinates x and y are horizontal, z is directed downwards. The system is used to describe the motion of the ship, the water surface, and the motion of water particles by the gradient of a flow potential.
- A ship-fixed coordinate system with coordinates $\underline{x}$ (longitudinal to the bow), $\underline{y}$ (to starboard), $\underline{z}$ (in ship-fixed downward direction). It is used to describe the ship shape and its mass distribution.
- An intermediate system $\tilde{x},\tilde{y},\tilde{z}$ which participates in the horizontal translations and the yaw motion of the ship, but not in heave, roll and pitch motion. It is used to generate the free-surface panel mesh.

The relation between a vector $\vec{x} = (x,y,z)$ expressed in inertial coordinates and the same vector $\underline{\vec{x}} = (\underline{x},\underline{y},\underline{z})$ expressed in ship-fixed coordinates, is

$$\vec{x} = \vec{u} + T\underline{\vec{x}}, \tag{1}$$

where $\vec{u} = (u_x,u_y,u_z)$ is the translation vector (position vector of the ship-fixed coordinate origin), and T is the matrix representing the combined rotations φ (heel), θ (pitch) and ψ (yaw):

$$T = T_\psi T_\theta T_\varphi. \tag{2}$$

Here T_φ is the matrix representing a right-hand rotation by angle φ about the x axis:

$$T_\varphi = \begin{pmatrix} 1 & 0 & 0 \\ 0 & \cos\varphi & -\sin\varphi \\ 0 & \sin\varphi & \cos\varphi \end{pmatrix}. \tag{3}$$

Correspondingly, T_θ is the matrix for pitch rotation; it is obtained from T_φ by cyclic permutation of rows and columns (to the right and down) and substituting φ by θ. T_ψ is obtained in the same way from T_θ. The corresponding relations involving vectors expressed in the intermediate system are

$$\vec{\tilde{x}} = (0,0,u_z)^T + T_\theta T_\varphi\, \underline{\vec{x}} \tag{4}$$

and

$$\vec{x} = (u_x,u_y,0)^T + T_\psi \vec{\tilde{x}}. \tag{5}$$

3 SUBDIVISION OF THE FLOW POTENTIAL

The total flow potential $\phi(\vec{x},t)$ and the free-surface deformation $\zeta(x,y,t)$ are combined from

- $\phi_s,\ \zeta_s$ of the exciting regular wave or irregular seaway. In case of regular waves, third-order Stokes waves are used; and
- $\phi_d,\ \zeta_d$ of the disturbance caused by the body.

ϕ_s and ζ_s are assumed to be known; ϕ_d and ζ_d will be determined numerically.

The subdivision of ϕ and ζ is essential for solving a common problem of numerical computations of free surface flows: wave reflections at the outer boundary of the computational domain. Here only reflections of the disturbance waves must be eliminated. Their amplitudes tend to zero with increasing distance from the hull and are much smaller than amplitudes of the total waves; thus inaccuracies produced by damping of the disturbance waves are much smaller than those produced by damping of the combined waves.

4 PANEL MESHES AND TIME DERIVATIVES

To allow possible extreme variations of the waterline with time, the free surface panel mesh is generated anew at each time step. To generate also a body panel mesh up to the actual waterline reliably at each time step appears difficult and time consuming. Therefore a constant body panel mesh moving with the body is used here. It extends at least up to the line of maximum immersion. (If non-smooth obstacles above the weather deck like hatches, containers and superstructures are immersed, the applicability of a panel method for ships with forward speed appears questionable.)

The fluid pressure depends on the partial time derivative (i.e. at points fixed in the inertial system) of the flow potential. To determine this derivative from finite differences between ϕ values at successive time steps would be inaccurate, especially at the water surface where the panel mesh may change extremely between time steps. It appears much more accurate to directly compute $\dot{\phi}$ from its boundary conditions, as proposed by Bandyk and Beck [1]. As also $\dot{\phi}$ satisfies the Laplace equation, the same panel method can be used to determine ϕ and $\dot{\phi}$, and even the same panel mesh and influence matrix are applicable to determine both ϕ and $\dot{\phi}$.

In the following, partial time derivatives $\partial/\partial t$ (at constant points $\vec{x}$) are designated by dots like in $\dot{\phi}$, whereas time derivatives at points moving with the mesh (within a single time step) are designated by d/dt. Both operators are related by

$$\frac{d}{dt} = \frac{\partial}{\partial t} + \vec{v}\cdot\nabla, \tag{6}$$

where $\vec{v}$ is the velocity of the mesh point in the inertial system.

5 BODY BOUNDARY CONDITION

To suppress any flow through the hull, the condition

$$(\nabla\phi - \vec{v})\vec{n} = 0 \tag{7}$$

must be satisfied for points $\vec{x}$ on the wetted ship surface. $\vec{v}$ is the body velocity at $\vec{x}$, and $\vec{n}$ a normal vector on the hull at $\vec{x}$.

The time derivative of (7) at body-fixed points is the boundary condition for $d\phi/dt$:

$$\left(\frac{d\nabla\phi}{dt} - \frac{d\vec{v}}{dt}\right)\vec{n} + (\nabla\phi - \vec{v})\frac{d\vec{n}}{dt} = 0. \tag{8}$$

The time derivatives in this equation are:

$$\frac{d\nabla\phi}{dt} = \nabla\dot{\phi} + (\nabla\nabla\phi)\vec{v}. \tag{9}$$

$\nabla\nabla\phi$ is the Hesse matrix (matrix of second partial derivatives) of ϕ. The time derivative of (1) results in

$$d\vec{x}/dt = \vec{v} = \dot{\vec{u}} + \dot{T}\underline{\vec{x}} = \dot{\vec{u}} + \vec{\omega}\times T\underline{\vec{x}}, \tag{10}$$

where $\vec{\omega}$ is the angular velocity of the body. The time derivative of this equation gives

$$d\vec{v}/dt = \ddot{\vec{u}} + \vec{\omega}\times(\vec{\omega}\times T\underline{\vec{x}}) + \dot{\vec{\omega}}\times T\underline{\vec{x}}. \tag{11}$$

The last derivative in (8) is

$$d\vec{n}/dt = \vec{\omega} \times \vec{n}. \tag{12}$$

Inserting $\phi = \phi_s + \phi_d$ into the body boundary conditions (7) and (8) gives the required boundary conditions for the potentials ϕ_d and $d\phi_d/dt$:

$$\nabla\phi_d \vec{n} = (\vec{v} - \nabla\phi_s)\vec{n}; \tag{13}$$

$$\nabla \frac{d\phi_d}{dt}\vec{n} = -\nabla\dot{\phi}_s\vec{n} - \vec{v}(\nabla\nabla\phi_s)\vec{n} + (\vec{v} - \nabla\phi_d - \nabla\phi_s)\frac{d\vec{n}}{dt} + \frac{d\vec{v}}{dt}\vec{n}. \tag{14}$$

In many panel methods, computing the Hesse matrix $\nabla\nabla\phi$ of the flow potential causes problems because the method may converge (for decreasing panel size) to correct first derivatives of the potential, but – due to insufficient smoothness – not to correct second derivatives. In (14), however, there are no such problems because $\nabla\nabla\phi_s$ is accurately computed from the formula for ϕ_s, whereas the Hesse matrix of ϕ_d is not required.

The last term in (14) involves $d\vec{v}/dt$, which – as shown by (11) – contains the translational and rotational body accelerations $\ddot{\vec{u}}$ and $\dot{\vec{\omega}}$. As these are not known initially when dealing with a new time step, $d\phi_d/dt$ is subdivided into seven contributions:

$$\frac{d\phi_d}{dt} = \phi_1\ddot{u}_x + \phi_2\ddot{u}_y + \phi_3\ddot{u}_z + \phi_4\dot{\omega}_x + \phi_5\dot{\omega}_y + \phi_6\dot{\omega}_z + \phi_7. \tag{15}$$

The potentials ϕ_1 until ϕ_6 will be used to determine the added mass and inertia matrix, whereas ϕ_7 comprises all contributions to $d\phi_d/dt$ which are not proportional to the body accelerations, e.g. diffraction and effects of body angular velocity. Corresponding to this subdivision, the following body boundary conditions are prescribed for ϕ_1 to ϕ_6:

$$\nabla\phi_1\vec{n} = n_x; \quad \nabla\phi_2\vec{n} = n_y; \quad \nabla\phi_3\vec{n} = n_z; \tag{16}$$

$$\nabla\phi_4\vec{n} = (T\vec{\underline{x}} \times \vec{n})_x; \quad \nabla\phi_5\vec{n} = (T\vec{\underline{x}} \times \vec{n})_y; \quad \nabla\phi_6\vec{n} = (T\vec{\underline{x}} \times \vec{n})_z. \tag{17}$$

When the subdivision (15) is inserted into the body boundary condition (14), many terms cancel because of the above boundary conditions for ϕ_1 to ϕ_6. The remaining rest is the body boundary condition for ϕ_7:

$$\nabla\phi_7\vec{n} = -\nabla\dot{\phi}_s\vec{n} - \vec{n}(\nabla\nabla\phi_s)\vec{v} + (\vec{v} - \nabla\phi_d - \nabla\phi_s)\frac{d\vec{n}}{dt} + [\vec{\omega} \times (\vec{\omega} \times T\vec{\underline{x}})]\vec{n}. \tag{18}$$

6 FREE SURFACE BOUNDARY CONDITIONS

If p is the difference between fluid and air pressure (the latter is approximated as constant), at the water surface $z = \zeta(\vec{x},t)$ Bernoulli's equation requires:

$$\frac{p}{\rho} = g\zeta - \dot{\phi} - \frac{1}{2}(\nabla\phi)^2 = 0. \tag{19}$$

Thus we have a Dirichlet-type free surface boundary condition for $\dot{\phi}$:

$$\dot{\phi} = g\zeta - \frac{1}{2}(\nabla\phi)^2. \tag{20}$$

The kinematic condition states that a fluid particle at the free surface will stay at the free surface:

$$\frac{D}{Dt}(z - \zeta) = (\frac{\partial}{\partial t} + \nabla\phi\nabla)(z - \zeta) = -\dot{\zeta} + \phi_z - \nabla\phi\nabla\zeta = 0, \tag{21}$$

from which follows:

$$\dot{\zeta} = \phi_z - \nabla\zeta\nabla\phi. \tag{22}$$

Inserting $\zeta = \zeta_s + \zeta_d$ into the boundary conditions (20) and (22) gives

$$\dot{\phi}_s + \dot{\phi}_d = g(\zeta_s + \zeta_d) - \frac{1}{2}(\nabla\phi_s + \nabla\phi_d)^2; \tag{23}$$

$$\dot{\zeta}_s + \dot{\zeta}_d = \phi_{s,z} + \phi_{d,z} - (\nabla\zeta_s + \nabla\zeta_d)(\nabla\phi_s + \nabla\phi_d). \tag{24}$$

The incident waves ϕ_s, ζ_s alone should satisfy both free surface conditions. But because we will use only approximations for ϕ_s and ζ_s (e.g., a 3rd order Stokes wave or a superposition of Airy waves), there remain errors which, when using the conditions (23) and (24), constitute forcing terms for ϕ_d, ζ_d also far from the body. This contradicts the decrease of the disturbance waves ϕ_d, ζ_d to zero at the outer boundary of the free surface panel mesh. Thus, to avoid these forcing terms, the dynamic condition for ϕ_s alone is subtracted from (23), and the kinematic condition for ζ_s alone from (24). The effect of this is: Errors of the assumed incident waves regarding their free surface boundary conditions are not cancelled by ϕ_d and ζ_d, but remain in the final solution. Whether these errors are relevant for the responses of interest can be tested by using more accurate formulae for the incident waves, e.g. according to [2].

The conditions for ϕ_s and ζ_s hold at ζ_s, whereas the conditions for ϕ_d and ζ_d hold at $\zeta_s + \zeta_d$. To take account of this difference, a first-order Taylor expansion for ϕ_s over z is applied to convert the free surface conditions for ϕ_s and ζ_s to the position $\zeta_s + \zeta_d$ before subtracting these conditions from (23) and (24). This results in the following free surface boundary conditions for $\dot{\phi}_d$ and $\dot{\zeta}_d$:

$$\dot{\phi}_d = \zeta_d(g - \dot{\phi}_{s,z} - \nabla\phi_s\nabla\phi_{s,z}) - \nabla\phi_s\nabla\phi_d - \frac{1}{2}(\nabla\phi_d)^2 + \frac{1}{2}(\nabla\phi_{s,z}\zeta_d)^2. \tag{25}$$

$$\dot{\zeta}_d = \phi_{d,z} + \phi_{s,zz}\zeta_d - \nabla\zeta_s\nabla\phi_d - \nabla\zeta_d(\nabla\phi_s + \nabla\phi_d) - \nabla\zeta_s\nabla\phi_{s,z}\zeta_d. \tag{26}$$

At a point moving with the free surface panel mesh (local speed $\dot{\vec{x}}$) we have

$$\frac{d\phi_d}{dt} = \dot{\phi}_d + \nabla\phi_d\dot{\vec{x}} = \phi_1\ddot{u}_x + \phi_2\ddot{u}_y + \phi_3\ddot{u}_z + \phi_4\dot{\omega}_x + \phi_5\dot{\omega}_y + \phi_6\dot{\omega}_z + \phi_7 + \nabla\phi_d(\dot{\vec{x}} - \vec{v}), \tag{27}$$

where the last expression follows from (15). The last term results from the fact that in (15) $d\phi_d/dt$ holds for a point with fixed $\vec{x}$ whereas here it refers to a point moving with the free-surface mesh. The condition is satisfied by choosing on the free surface

$$\phi_i = 0 \quad \text{for} \quad i = 1 \quad \text{to} \quad 6, \tag{28}$$

and

$$\phi_7 = \dot{\phi}_d + \nabla\phi_d\vec{v}. \tag{29}$$

The conditions for ϕ_1 to ϕ_6 correspond to an added mass matrix for infinite frequency. This is no approximation, because the condition (27) is exactly satisfied by the rest potential ϕ_7.

Like for the acceleration potentials ϕ_1 to ϕ_7, on the free surface we have a Dirichlet boundary condition also for ϕ_d. Its values follow from the time integration (within the current time step) of ϕ_d using $d\phi_d/dt$. The value at the beginning of each time step must be interpolated from the end value of the previous time step, using interpolation between previous and current mesh.

The surface deformation ζ_d is determined correspondingly by time integration of $d\zeta_d/dt$. The latter is determined as

$$d\zeta_d/dt = \dot{\zeta}_d + \nabla\zeta_d\dot{\vec{x}}, \tag{30}$$

where $\dot{\zeta}_d$ is given by (26).

7 TRANSOM CONDITION

If a transom is immersed to a depth exceeding U^2/g, the transom is assumed to be wetted and treated like other parts of the hull. For less immersion, the transom is assumed dry, and the pressure at the hull panels immediately in front of the transom is forced to air pressure.

If U-shaped transverse sections at the aft end of the hull cause a very blunt waterline, the case is treated like a dry transom.of submergence zero, and the free surface panels immediately behind the end of the waterline are assumed to be horizontal.

8 RADIATION CONDITION

Usually one wants to model the response of a body due to a given incident wave and the accompanied disturbance by the body. The body and free surface boundary conditions, however, do not exclude the presence of other external waves. They could stem from the starting process of the simulation, or they may be accumulating from numerical errors during long simulations. To avoid such unwanted waves, damping must be added. Here wave damping is produced by assuming a higher or lower pressure at the free surface where it moves upward or downward, respectively, in the intermediate coordinate system. This results in an additional term

$$\delta_w c \, d\zeta_d/dt \tag{31}$$

on the right-hand side of (25). c is the phase velocity of the wave or the seaway at its significant frequency, and δ_w is a non-dimensional parameter. In other publications, wave damping is applied in a 'damping zone' near to the outer boundary of the computational domain. Numerical tests showed, however, that a constant damping parameter δ_w (for instance $\delta_w = 0.4$) gives superior results. This may be understood from the fact that waves are reflected not only at the outer boundary, but partially also at the lines of constant damping parameter if damping changes normally to that line.

Waves due to forward speed of a ship, which travel along with it, are not damped by the term (31). These waves should have a far field only behind, not in front of the disturbance causing them. That is attained here by using the Dawson [3] operator: When determining $\nabla\phi_d$ or $\nabla\zeta_d$ at a point P, the derivative in the ship's longitudinal direction $\tilde{x}$ is estimated as that of an interpolating 4th order polynomial passing through the function values at P and at the three next mesh points in front of P. All together 4 points suffice because the interpolating polynomial used by Dawson lacks the 3rd-order term:

$$f(\tilde{x}) = a_0 + a_1(\tilde{x}-\tilde{x}_P) + a_2(\tilde{x}-\tilde{x}_P)^2 + a_4(\tilde{x}-\tilde{x}_P)^4. \tag{32}$$

To use only upstream points avoids that disturbances generate waves far upstream. In other directions and for bodies without forward speed, spacial derivatives of ϕ_d and ζ_d are determined as described later.

9 NUMERICAL METHOD TO SATISFY THE BODY BOUNDARY CONDITION

As an alternative to the most-used panel method, a variant of it called patch method [4] is used here. Whereas panel methods use distributed sources and satisfy the boundary condition at certain points, the patch method uses point sources and satisfies the boundary condition in the average over each panel. Here, on the body a mesh of triangular panels is used (Fig. 1). Point sources may be located on the fluid boundary, but usually they are posed a suitable distance (substantially less than the triangle size and the local radius of curvature) behind the hull within the body. Gradients of a source flow are not determined as analytic derivatives; instead, the gradient, averaged over a panel, is determined from the potential at the three vertices (giving the tangential components of the gradient) and from the flux through the panel (giving the normal component). The potential itself, averaged over the panel, is usually approximated as the average of its value at the midpoints of the panel sides, which are Gauß integration points for a triangular region. (As an alternative, an analytical formula may be used.)

For partly submerged panels, the ratio r of the submerged area to the total panel area is used to decrease the strength of the source next to the panel by factor r (by dividing the element on the main diagonal of the influence matrix by $1/r$). Fully emerged body panels are eliminated from the equation system. Within each time step, the change of r is under-relaxed to avoid oscillations of r. To take account of the time dependence of r, the term

$$\nabla \frac{1}{|\vec{x}-\vec{x}_{qi}|} \, \frac{-q_i}{r_i^2} \, \frac{dr_i}{dt} \, \vec{n} \tag{33}$$

must be added on the right-hand side of the discretised form of the boundary condition (18).

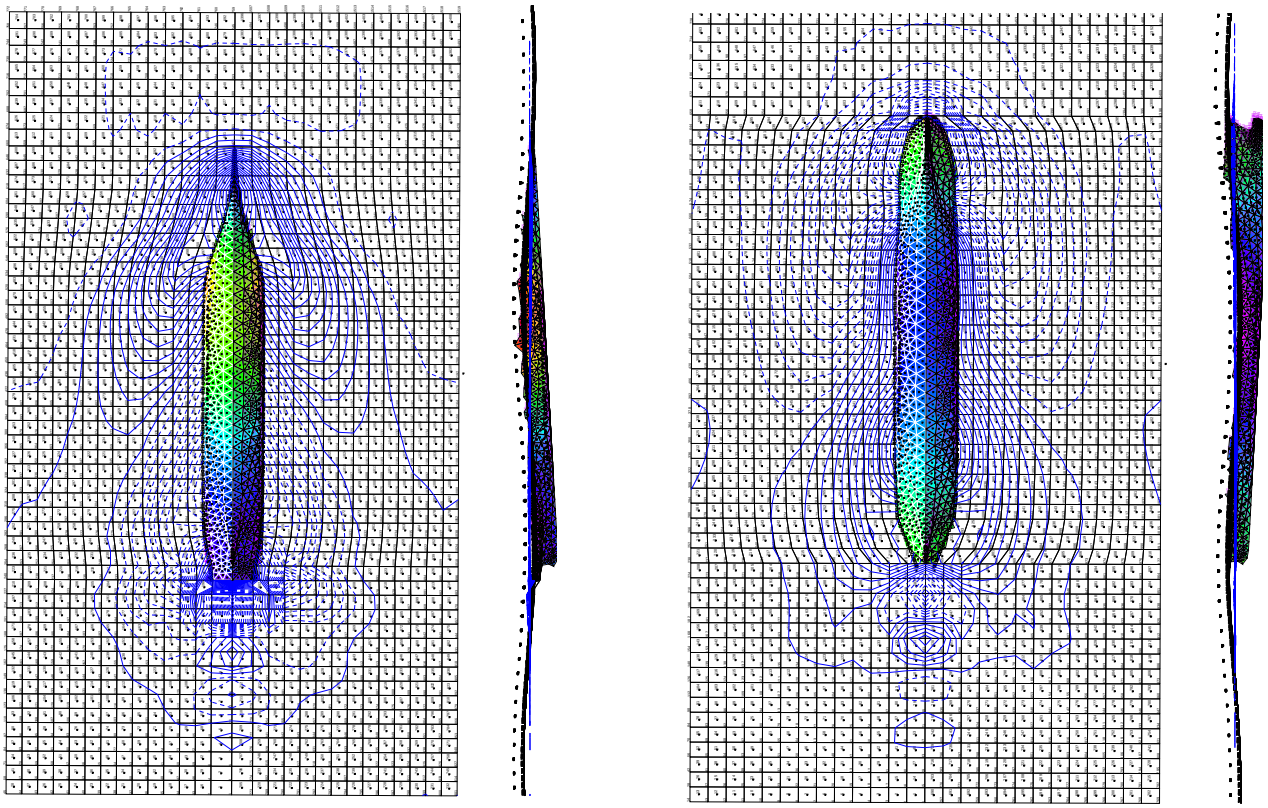

Figure 1: Panel mesh of the WILS containership [5] at two instants in regular head waves of 8m height. Colours on hull panels code the dynamic pressure. Contour lines show the surface deformation ζ_d, excluding the exciting waves ζ_s.

10 NUMERICAL METHOD TO SATISFY THE FREE SURFACE CONDITIONS

At the beginning of each time step, the panel mesh on the free surface is generated around the waterline. As the nearly horizontal hull in the stern region of most modern ships may cause highly curved or even discontinuous waterline shapes, the aft part of the waterline is approximated by a straight line to avoid irregular panel meshes. During each time step, waterline changes are taken into account by appropriate mesh deformations in the intermediate coordinate system. In the inertial system the mesh is moving also according to the change from intermediate to inertial coordinate system.

For each quadrilateral free surface panel a point source is arranged approximately one panel length above the free surface. A single additional source is arranged higher above the midship section. It is required to take account of another condition for in-stationary free surface flows: The sum of all source strengths must be zero to attain the correct far-field behaviour of the fluid pressure.

Gradients averaged over a rectangular patch are determined by subdividing the patch into two triangles, for which the procedure described before is used. For ships with forward speed, the result is modified using the Dawson method.

For each free surface panel, the kinematic boundary condition gives the (panel-averaged) vertical speed of the free surface. For each mesh point the average value of the (normally four) surrounding panels is used to update the vertical coordinate of the mesh point using the 4th order Runge-Kutta method. An exception are points on the waterline: To avoid irregularities like spray and breaking waves, the surface height at the waterline is extrapolated from the next two mesh points besides the waterline.

The dynamic free-surface condition, on the other hand, gives the time derivative of the panel-averaged potentials ϕ_d. Again, the 4th order Runge-Kutta method is used to determine ϕ_d itself.

11 DETERMINATION OF SOURCE STRENGTHS

The velocity potential ϕ_d is combined from that of point sources:

$$\phi_d(\vec{x},t) = \sum_j \frac{-q_j(t)}{|\vec{x}-\vec{x}_{qj}|}, \tag{34}$$

where the sum comprises body sources, free surface sources and the additional single source. Corresponding formulae are used for the acceleration potentials ϕ_i, $i = 1$ to 7, however with different sets of source strengths $q_j^{(i)}$. The boundary conditions for each panel form a linear equation system having the same coefficient matrix for all 8 potentials, however with 8 different inhomogeneous vectors. The inhomogeneous vector for ϕ_7 can only be determined when the source strengths of ϕ_d are known. Therefore, at first an LU factorization of the coefficient matrix is made; then the source strengths for ϕ_d and ϕ_1 to ϕ_6 are determined; the q_j allow to compute the inhomogeneous vector for ϕ_7; and finally the source strengths of ϕ_7 are determined. This is done using subroutines of the Linear Algebra Package (LAPACK) which proved to be very efficient. Iterative solvers are not applicable here both because of the bad condition number of the system, and because we must solve for 8 different inhomogeneous vectors.

12 DETERMINATION OF BODY FORCE AND MOMENT

The pressure force F_p on the body is added from contributions of all fully or partly submerged body panels:

$$\vec{F}_p = \sum_i p_i \vec{n}_i r_i. \tag{35}$$

Here the normal vector $\vec{n}_i$ of panel i is scaled such that it points into the body, and that its absolute value is the panel area. The pressure difference to the air pressure p is

$$p = \rho\left(gz - \dot{\phi} - \frac{1}{2}(\nabla\phi)^2\right) = \rho\left(gz - \phi_1\ddot{u}_x ... - \phi_6\dot{\omega}_z - \phi_7 + \nabla\phi_d\vec{v} - \dot{\phi}_s - \frac{1}{2}(\nabla\phi)^2\right). \tag{36}$$

F_p is subdivided into contributions independent and dependent from the accelerations:

$$\vec{F}_p = \vec{F}_0 - A_u \begin{pmatrix} \ddot{\vec{u}} \\ \dot{\vec{\omega}} \end{pmatrix}. \tag{37}$$

Here

$$\vec{F}_0 = \sum_i \rho\left(gz_i - \phi_{7i} + \nabla\phi_{di}\vec{v}_i - \dot{\phi}_{si} - \frac{1}{2}(\nabla\phi_i)^2\right)\vec{n}_i r_i, \tag{38}$$

and A_u is the upper half of the 6 by 6 added mass matrix. Its elements in rows 1 to 3 of column j are

$$A_{1:3,j} = \rho\sum_i \phi_j \vec{n}_i r_i. \tag{39}$$

Correspondingly, the pressure moment about G is subdivided:

$$\vec{M}_p = \vec{M}_0 - A_l \begin{pmatrix} \ddot{\vec{u}} \\ \dot{\vec{\omega}} \end{pmatrix}, \tag{40}$$

where A_l is the lower half of the added mass matrix. $\vec{M}_0$ and the elements of A_l are determined by equations analogous to (38) and (39), however containing $(\vec{x}_i - \vec{x}_G) \times \vec{n}_i$ instead of $\vec{n}_i$.

To obtain the total force $\vec{F}$ and the moment $\vec{M}$ on the body, we have to add a residual force $\vec{F}_r$ and its moment $\vec{M}_r$. These stem from the following contributions:

- Weight force
- Viscous and other corrections, e.g. due to flow separation especially at the stern and the rudder
- Control forces. They can be used to keep, approximately, the planned speed and path, and are quantified by parameters of a PID control loop.
- Possibly wind and other external forces and moments

13 MOTION EQUATIONS

If $\vec{x}_G$ is the position of the center of gravity of (rigid) masses in ship-fixed coordinates, its acceleration follows from (11) as

$$\ddot{\vec{u}}_G = \ddot{\vec{u}} + \vec{\omega} \times (\vec{\omega} \times T\underline{\vec{x}}_G) + \dot{\vec{\omega}} \times T\underline{\vec{x}}_G. \tag{41}$$

From Newton's law

$$m\ddot{\vec{u}}_G = \vec{F} \tag{42}$$

together with (41) and (37) follows:

$$m[\ddot{\vec{u}} + \vec{\omega} \times (\vec{\omega} \times T\underline{\vec{x}}_G) + \dot{\vec{\omega}} \times T\underline{\vec{x}}_G] = \vec{F}_0 - A_{1:3,1:6} \begin{pmatrix} \ddot{\vec{u}} \\ \dot{\vec{\omega}} \end{pmatrix} + \vec{F}_r. \tag{43}$$

Body rotations are governed by the equation

$$\Theta\dot{\vec{\omega}} + \vec{\omega} \times \Theta\vec{\omega} = \vec{M} = \vec{M}_0 - A_l \begin{pmatrix} \ddot{\vec{u}} \\ \dot{\vec{\omega}} \end{pmatrix} + M_r, \tag{44}$$

where the right-hand expression follows from the subdivision of M into pressure (40) and residual moment. Θ is the inertia matrix of rigid body masses referring to G in inertial coordinates. It is determined from the time-invariant inertia matrix in ship-fixed coordinates, $\underline{\Theta}$, as

$$\Theta = T\underline{\Theta}T^T. \tag{45}$$

Equations (43) and (44) for translational and rotational motion will be combined to one matrix equation for the six accelerations. To that end, the vector product involving $\dot{\vec{\omega}}$ in (43) is written in index notation. For arbitrary 3-dimensional vectors $\vec{a} = (a_1, a_2, a_3)$ and $\vec{b} = (b_1, b_2, b_3)$ their vector product can be written as

$$\vec{a} \times \vec{b} = \varepsilon_{ijk} a_j b_k, \tag{46}$$

where ε_{ijk} are the elements of the Levi-Civita tensor: ε_{ijk} is 1 if ijk constitute an even permutation of (1,2,3); -1 for an odd permutation; and 0 if i, j, k are not all different. Using this notation, (43) and (44) can be combined into the matrix equation

$$\left[\begin{pmatrix} mE & m\varepsilon_{ijk}(T\underline{\vec{x}}_G)_k \\ 0 & T\underline{\Theta}T^T \end{pmatrix} + A \right] \begin{pmatrix} \ddot{\vec{u}} \\ \dot{\vec{\omega}} \end{pmatrix} = \begin{pmatrix} \vec{F}_0 + \vec{F}_r - m\vec{\omega} \times (\vec{\omega} \times T\underline{\vec{x}}_G) \\ \vec{M}_0 + \vec{M}_r - \vec{\omega} \times T\underline{\Theta}T^T\vec{\omega} \end{pmatrix}. \tag{47}$$

Here E is the 3 by 3 unit matrix, 0 the 3 by 3 zero matrix, and A the 6 by 6 added mass matrix. The rigid mass matrix on the left-hand side (in parentheses) may appear unusual. The reason is: Here moments and moments of inertia refer to the center of gravity G, but the translation $\vec{u}$ refers to the origin of the body-fixed coordinate system.

The 6 by 6 linear equation system (47) is solved for the accelerations $\ddot{\vec{u}}$ and $\dot{\vec{\omega}}$. Then $\dot{\vec{u}}$, $\vec{u}$ and $\vec{\omega}$ follow by Runge-Kutta time integration. The time derivatives of the rotation angles follow from $\vec{\omega}$ as

$$\begin{pmatrix} \dot{\varphi} \\ \dot{\theta} \\ \dot{\psi} \end{pmatrix} = \begin{pmatrix} \cos\psi/\cos\theta & \sin\psi/\cos\theta & 0 \\ -\sin\psi & \cos\psi & 0 \\ \tan\theta\cos\psi & \tan\theta\sin\psi & 1 \end{pmatrix} \vec{\omega} \tag{48}$$

(for $\theta < 90$ degrees). Finally, the rotation angles follow from $(\dot{\varphi}, \dot{\theta}, \dot{\psi})$ by Runge-Kutta integration.

14 VERIFICATION FOR HEAD WAVES

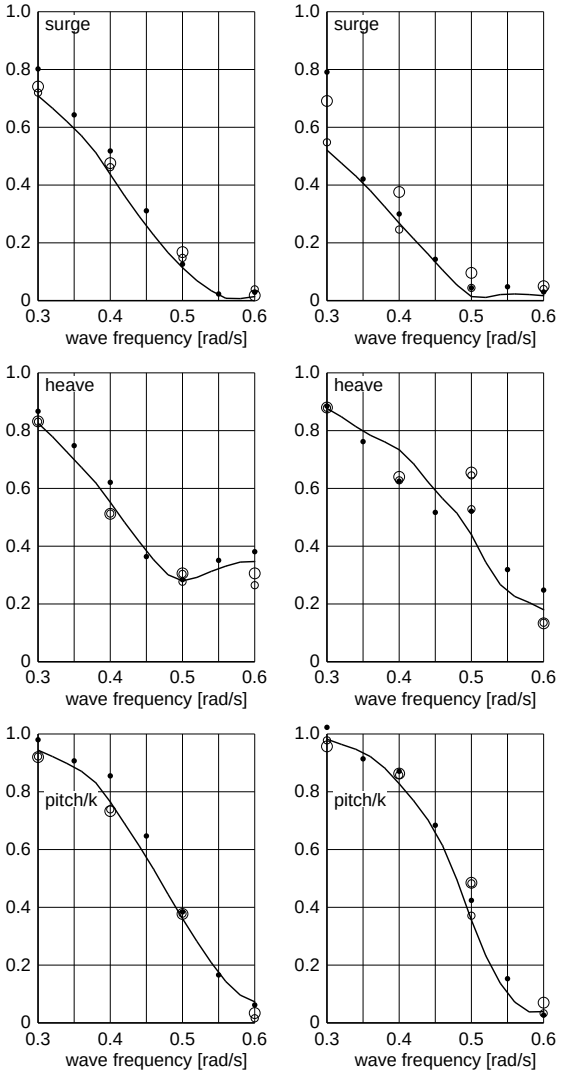

Figure 2: Linear transfer functions of surge, heave and pitch motions of the WILS containership in head waves for speeds 5 (left) and 15 knots (right). Curves: results of program GLRankine [5]; dots: results of model experiments by KRISO; circles: present method for different control force parameters. k = wave number.

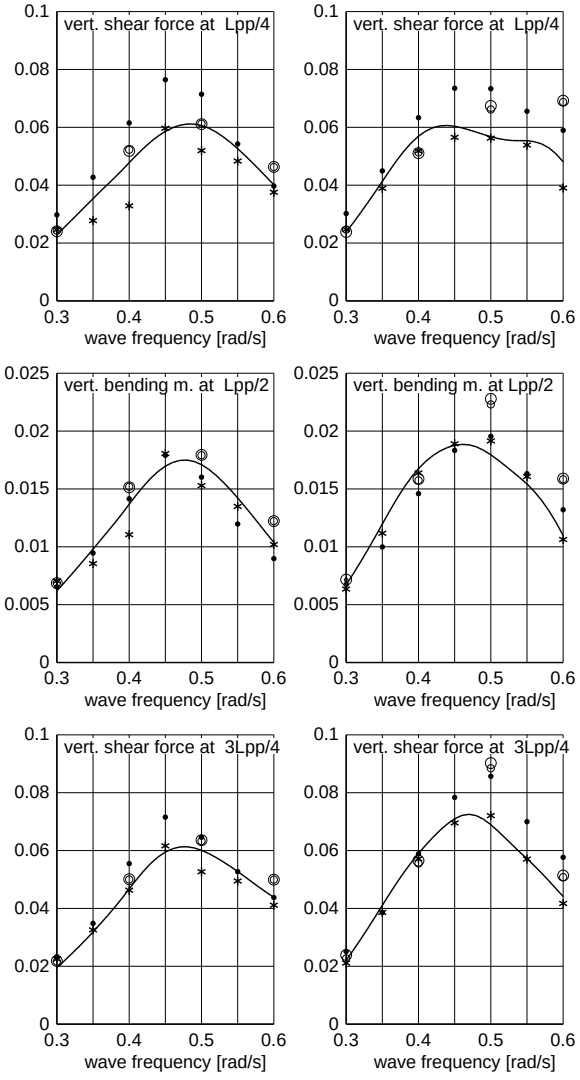

Figure 3: Fig. 3. Like Fig. 2, however for non-dimensional vertical shear force $F_z/\rho g L_{pp} B a$ at 1/4 and 3/4 L_{pp} (a = wave amplitude) and vertical bending moment $M_y/\rho g L_{pp}^2 B a$ at midship section. Asterisks for RANSE calculations [5].

Figs. 2 and 3 show results for the WILS containership ($L_{pp} = 286.3$m, $B = 40.3$m, $T = 13.05$m; [5]) in low-amplitude head waves. Fig. 4 corresponds to Fig. 3 for speed 5kn, however for waves of large amplitude.

15 VERIFICATION FOR QUARTERING WAVES

Again the WILS ship is investigated sailing with 5kn in quartering waves ($\mu = 60$ degrees). Simulations in oblique waves are much more difficult than those in head waves: They involve roll, in which restoring moments

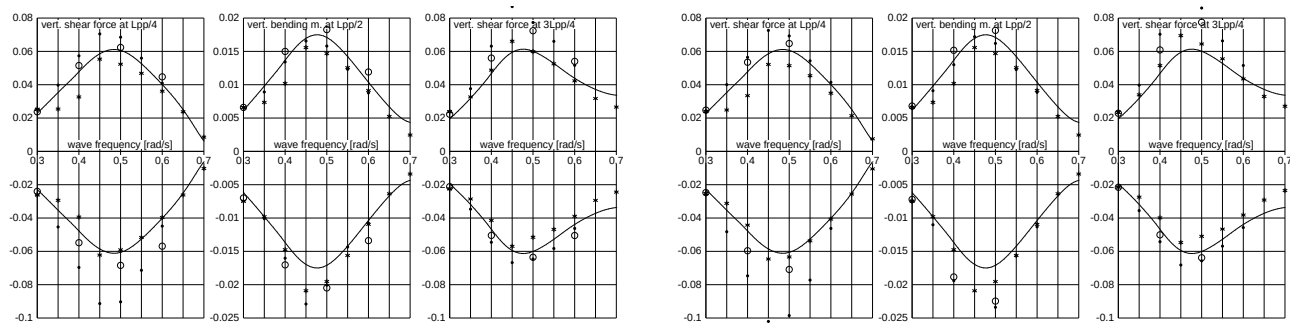

Figure 4: Maximum and minimum non-dimensional shear force $F_z/\rho g L_{pp} Ba$ and bending moment $M_y/\rho g L_{pp}^2 Ba$. WILS containership (5 knots) in head waves of 7m (left) and 10m (right) height. Curves: linear program GLRankine; dots: model experiments by KRISO; asterisks: RANSE calculations (all taken from [5]); circles: present method.

are small (typically $< 1\%$ of restoring in pitch); lift forces produced by hull and rudder must be taken into account; and control actions are needed to limit deviations from the intended speed and course, both in model experiments and in non-linear simulations.

Fig. 5 compares linear transfer functions of motions measured in model experiments by KRISO and computed by a linear Rankine panel method and the present method. Fig. 6 does the same for torsional and horizontal bending moments at midship section. Fig. 7 compares maximum and minimum wave-induced force and moment (3 components each) at midship section for small wave heights as well as 7m and 10m wave height.

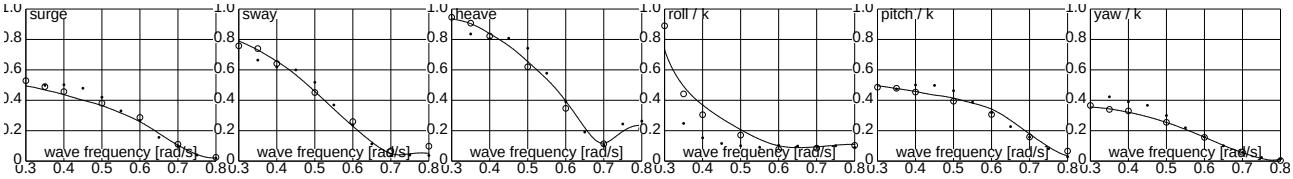

Figure 5: Linear transfer functions of motions of the WILS containership at 5kn in waves of $\mu = 60$degrees. Curves: results of program GLRankine [5]; dots: results of model experiments by KRISO; circles: present method.

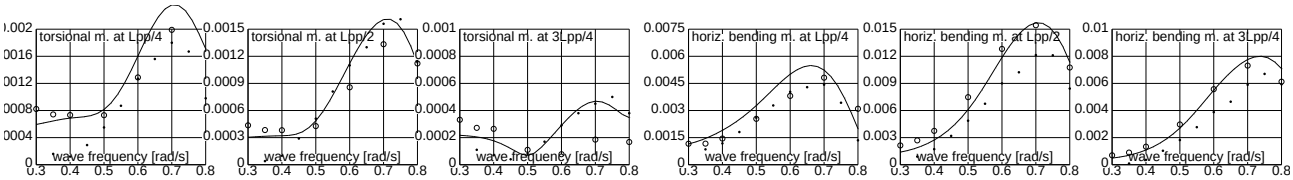

Figure 6: Like Fig. 5, however for the non-dimensional torsional moment $M_x/\rho g L_{pp}^2 Ba$ (left) and for the horizontal bending moment $M_z/\rho g L_{pp}^2 Ba$ (right)

16 CONCLUSIONS

The current work aimed at a computational method to predict seakeeping of actual ships in large-amplitude waves, which is of comparable accuracy to Euler- or RANSE-based computations, but requires much less computing time. On a single processor (5 years old), the present method needs, typically, between 30 and 150 times real time; thus, it is much faster than field methods solving Euler or RANS equations for the same application. Further it is shown that the accuracy of model experiments and of all tested kinds of computations is not high enough to demonstrate a superiority of any of these methods. In all tested cases, deviations between the results

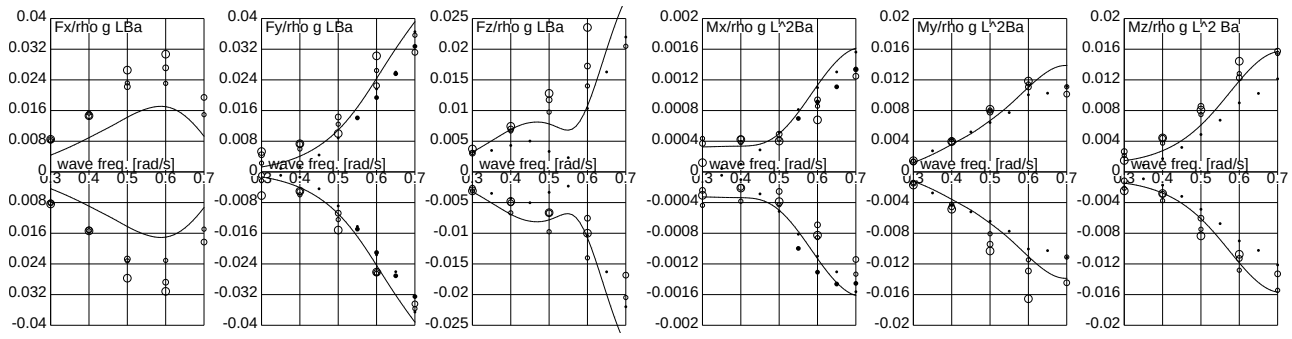

Figure 7: Non-dimensional maximum and minimum section force and moment at midship section for the WILS containership sailing with 5kn in waves of $\mu = 60$ degrees. Curves: linear Rankine source method [5]; small and larger dots: KRISO experiments with small amplitude and $a = 3.5$m [6]; small to large circles: present method for small a, $a = 3.5$m and $a = 5$m, respectively.

of the compared methods appear small enough to base technical decisions on them. Further developments of the present method are planned, e.g. for non-linear natural seaway, shallow water and manoeuvring in steep waves.

REFERENCES

[1] P. J. Bandyk and R. F. Beck. "The acceleration potential in fluid-body interaction problems". In: *Journal of Engineering Mathematics* 70.1 (2011), pp. 147–163.

[2] G. Ducrozet, F. Bonnefoy, D. Le Touzé and P. Ferrant. "HOS-ocean: Open-source solver for nonlinear waves in open ocean based on High-Order Spectral method". In: *Computer Physics Communications* 203 (2016).

[3] C. W. Dawson. "A Practical Computer Method for Solving Ship-Wave Problems". In: *Proceedings of Second International Conference on Numerical Ship Hydrodynamics* (1977), pp. 30–38.

[4] H. Söding. "A method for accurate force calculations in potential flow". In: *Ship Technology Research* 40 (1993), pp. 176–186.

[5] H. Söding, A. von Graefe, O. Moctar and V. Shigunov. "Rankine Source Method for Seakeeping Predictions". In: *Proceedings of the International Conference on Offshore Mechanics and Arctic Engineering - OMAE* 4 (2012).

[6] V. Shigunov, A. von Graefe and O. Moctar. "Calculation of Horizontal Sectional Loads and Torsional Moment". In: *Journal of Offshore Mechanics and Arctic Engineering* 137 (2015), pp. 021603–1.